Dendrochronologia 68 (2021) 125846

Contents lists available at ScienceDirect

Dendrochronologia

journal homepage: www.elsevier.com/locate/dendro

The variable climate response of Rocky Mountain bristlecone pine (*Pinus aristata* Engelm.)

William Lazar Tintor [a,b,*], Connie A. Woodhouse [a,b]

[a] School of Geography, Development and Environment, University of Arizona, Tucson, AZ, 85721, USA
[b] Laboratory of Tree-Ring Research, University of Arizona, Tucson, AZ, 85721, USA

ARTICLE INFO

Keywords:
Pinus aristata
Rocky Mountains
Tree growth
Climate response
Temperature sensitivity

ABSTRACT

Recent increases in temperature over the semi-arid western United States have been shown to exacerbate drought, reducing streamflow, and increasing stress on ecosystems. Our understanding of the role temperature played during drought in the more distant past is far from complete. While numerous tree-ring proxy records of moisture provide evidence for past extreme droughts in this region, few contemporaneous tree-ring proxy records of temperatures exist. This limits our ability to evaluate the variable influence of temperature on drought over past centuries and to contextualize the present interplay of moisture and temperature during more recent drought events. It is also important to understand the complexity of climatic interactions that produced drought under natural variability prior to evaluating the potential impacts of future climate change. In response to this knowledge gap, we undertook the first extensive evaluation of climate sensitivity in Rocky Mountain bristlecone pine (*Pinus aristata* Engelm.), focusing on the potential for developing new multi-century proxy records of both temperature and precipitation. We isolated dominant patterns of growth variability among trees from ten ring-width datasets across the Southern Rocky Mountains of Colorado and New Mexico and assessed their response to climate. We utilized both an empirical orthogonal function (EOF) analysis and a modified form of hierarchical cluster analysis to produce time series representing growth patterns in *P. aristata*. The results indicate a widespread June drought stress signal with a high potential for multi-millennial reconstruction. We also found a positive minimum temperature response during late summer, evident only at lower frequency and co-occurring at locations with the June drought stress signal. The potential for temperature reconstruction will require further investigation into the physiological linkages between *P. aristata* and climate variability. The presence of multiple climate responses within *P. aristata* sampling sites highlights the need for particular care when including *P. aristata* in regional climate reconstructions.

1. Introduction

Tree-ring reconstructions of precipitation and streamflow in the semi-arid western U.S. provide an expanded framework for contextualizing both the severity of current droughts and the impact of predicted climate change over the next century (Meko and Woodhouse, 2011). In this region, an abundance of tree-ring based reconstructions exists for streamflow (e.g. Meko et al., 2007; Woodhouse et al., 2012, 2006), precipitation (e.g. D'Arrigo and Jacoby, 1991), and Palmer Drought Severity Index (PDSI) (e.g. Cook et al., 2004). These tree-ring reconstructions show that past "megadroughts" were of a duration and severity unlike any experienced in our limited window of modern scientific record keeping (Woodhouse and Overpeck, 1998). Climate modeling predicts intensified droughts in the semi-arid western U.S. due to an increase in temperature and decrease in precipitation (Jones and Gutzler, 2016), although precipitation trends are prone to higher uncertainty (Deser et al., 2014). In recent decades, warming alone has exacerbated moisture deficits, increasing the severity of droughts and impacting streamflow on the Upper Colorado River (Udall and Overpeck, 2017; Woodhouse et al., 2016) and the Rio Grande (Chavarria and Gutzler, 2018; Lehner et al., 2017). With mid-range climate change scenarios predicting a 2.7 °C increase in average annual temperature by 2100 for the semi-arid western U.S. (Gonzalez et al., 2018) the impacts on water supply from warming are likely to continue. Revealing how temperature interacted with droughts over past centuries to millennia using tree-ring based climate reconstructions could improve our

* Corresponding author at: School of Geography, Development and Environment, University of Arizona, Tucson, AZ, 85721, USA.
E-mail address: wtintor@email.arizona.edu (W.L. Tintor).

https://doi.org/10.1016/j.dendro.2021.125846
Received 20 November 2020; Received in revised form 6 May 2021; Accepted 16 May 2021
Available online 20 May 2021

understanding of how temperatures may influence drought severity in a warmer future.

Despite the potential influence of temperature on past droughts, there is a deficit in annual tree-ring based temperature reconstructions for the region. A recent survey of Common Era proxy records found only ten temperature-sensitive tree-ring chronologies in the states of Arizona, Colorado, New Mexico, and Utah (Emile-Geay et al., 2017). Efforts to produce a comprehensive regional temperature reconstruction in the semi-arid western U.S. have been limited due to a lack of temperature-sensitive tree-ring chronologies, and most recently, a lack of updated chronologies. Fritts and Lough (1985) produced the first tree-ring based temperature reconstruction for this region, expanding on previous work that produced a relative index of past temperature variation (Blasing and Fritts, 1976; LaMarche and Stockton, 1974). Briffa et al. (1992) developed the first regional latewood density reconstruction of temperature for a gridded network that included the semi-arid western U.S. In the years since, several spatially limited temperature reconstructions have been produced for the Sierra Nevada (Graumlich, 1993), the southern Colorado Plateau (Salzer and Kipfmueller, 2005), the Great Basin (Salzer et al., 2009), and the Southern Rocky Mountains (Berkelhammer and Stott, 2012). Relative to the number of regionally developed precipitation and moisture reconstructions, temperature reconstructions are far outnumbered. With a limited set of temperature reconstructions available, a comparison between past droughts and temperature remains difficult.

Rocky Mountain bristlecone pine (*Pinus aristata* Engelm.) may provide an additional resource for this temperature reconstruction deficit. The related Great Basin bristlecone pine (*Pinus longaeva* D.K. Bailey) has been widely studied due to its 5000-year lifespan (Schulman, 1954), potential for climate reconstruction (Salzer et al., 2009), and preservation of remnant wood dating to the early Holocene (Salzer et al., 2019). While *P. longaeva* has been used for both annual precipitation (Knight et al., 2010) and temperature reconstructions (Salzer et al., 2009), research has indicated that inter-mixture of both precipitation and temperature signals is common within a *P. longaeva* sampling site due to topographic microclimates (Bunn et al., 2011) and proximity to upper tree line (Salzer et al., 2014b). Disentangling the mixed signals has involved cluster analysis (Tran et al., 2017), experimental temperature sensors (Bruening et al., 2017), and simulated tree-ring proxy growth models (Bunn et al., 2018).

Despite its extreme longevity (over 2500 years (Brunstein and Yamaguchi, 1992)) and natural habitat within major Southwest headwaters (i.e. Rio Grande and Arkansas River), *P. aristata* has not received the same level of investigation for climate sensitivity as *P. longaeva*. Limited research exists for *P. aristata* (Brunstein and Yamaguchi, 1992; Ferguson and Graybill, 1983; Krebs, 1973; LaMarche and Stockton, 1974), with only two precipitation proxy records (Routson et al., 2011; Woodhouse et al., 2011) and one temperature reconstruction (Salzer and Kipfmueller, 2005). Until now, no study has systematically examined the potential for *P. aristata* as a proxy for both temperature and

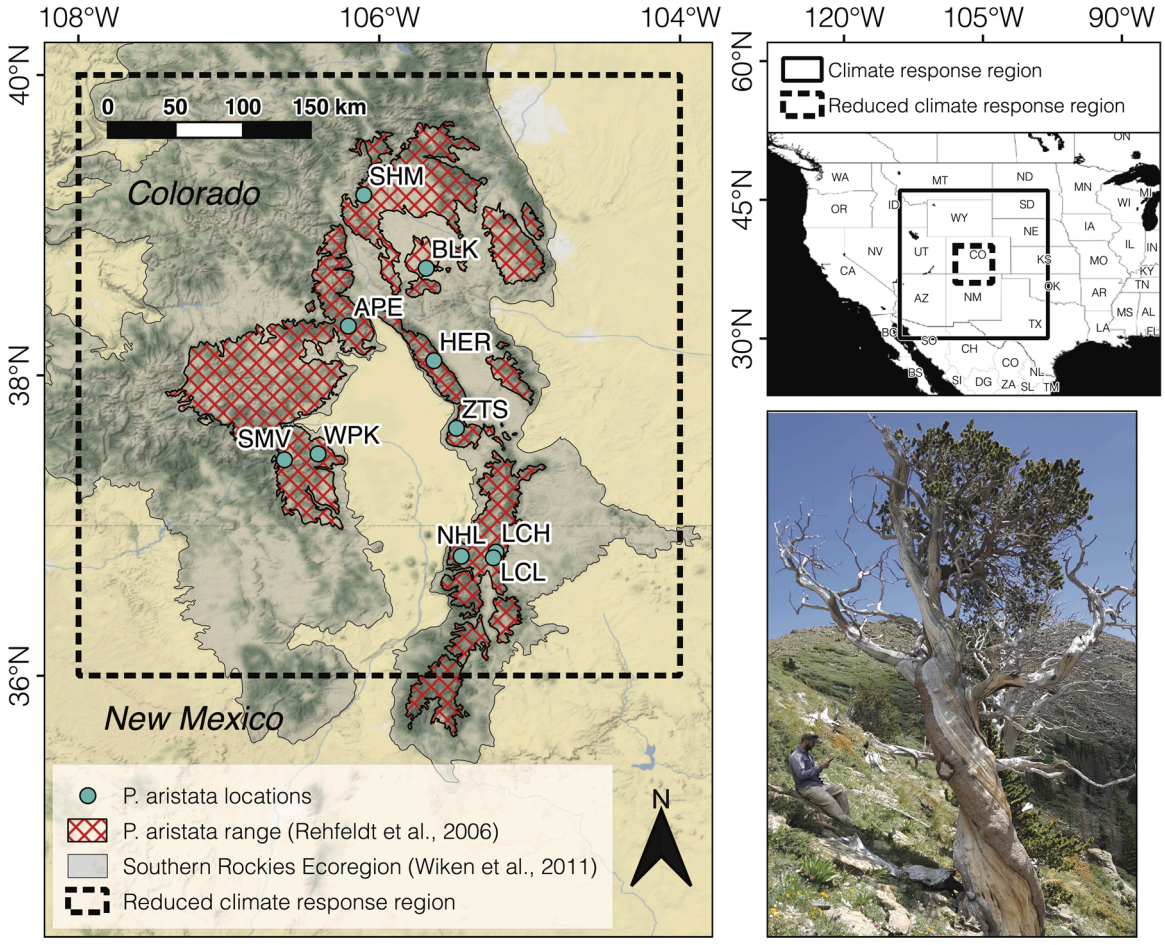

Fig. 1. Left panel: Locations of *P. aristata* sampling sites used in this study, within the estimated range of *P. aristata* (Rehfeldt et al., 2006) and the Southern Rockies Ecoregion (Wiken et al., 2011). Location three letter codes correspond to sampling site codes in Table 1. **Upper right panel:** Regions used for climate/tree-growth correlations. The climate response region (solid line) shows the area used to generate correlation field maps while the dashed line box represents a reduced response region used to calculate correlations between tree growth and climate at each PRISM grid point within this box. **Lower right panel:** >500 year-old *P. aristata* near upper tree line at the Hermit Lake collection site with narrow strip bark growth and reduced crown canopy.

moisture. A better understanding of the characteristics of *P. aristata* climate signals may improve this species' potential as a multi-millennia climate record, providing new regional temperature reconstructions and improving our understanding of past hydroclimates.

We undertook an evaluation of *P. aristata* chronologies across the Southern Rocky Mountains of Colorado and New Mexico (Fig. 1) to assess the variable response to climate between and within chronology sites. We used ten new and previously collected ring-width chronologies to answer the following questions:

1 What do the regional set of chronologies tell us about the *P. aristata* response to climate, and how it varies by location and site characteristics?
2 Within each sampling site, is the climate sensitivity consistent among trees that make up the site chronology or is there intra-site variability as documented in previous *P. longaeva* studies?
3 What is the potential for developing long moisture and/or temperature reconstructions from this set of data?

To isolate the dominant patterns of growth variability from the ring-width datasets, we used empirical orthogonal function (EOF, Preisendorfer and Mobley, 1988) analysis at both the chronology and the individual tree scales. We also used a modified form of hierarchical cluster analysis (Kipfmueller and Salzer, 2010) on a matrix of on-site correlations between the individual samples and the local climate to isolate a third set of tree-growth patterns. Following the isolation of growth signals, we constructed time series and correlated them with a regional gridded climate dataset to assess the relationship between *P. aristata* tree-ring growth patterns and climate. Finally, we evaluated the potential for these tree-ring growth data to be used in climate reconstructions.

2. Material and methods

2.1. Study area

This investigation is set in the Southern Rocky Mountains (Southern Rockies) of the continental United States. The Southern Rockies ecoregion is characterized by multiple ranges of high, steep mountains with peaks regularly exceeding 4000 m surrounded by valleys dropping below 2500 m (Wiken et al., 2011). This dramatic variation in topography controls all aspects of the regional climate, including temperature and precipitation. Temperature decreases with elevation, but local topography plays a role as well. Closed valleys surrounded by high peaks are susceptible to temperature inversions during the winter, with dense cold air sinking to the valley bottoms and reaching temperatures below −50 °C (Doesken et al., 2003). These inversions also occur at smaller spatial scales and diurnally. Precipitation is broadly controlled by elevation with annual totals ranging from 255 mm at lower elevation sites to 1750 mm on high mountains (Wiken et al., 2011). In addition, the steep topography produces rain shadow effects throughout the Southern Rockies, resulting in sharp contrasts in precipitation due to orographic effects. The majority of annual precipitation falls as snow (Wiken et al., 2011), resulting in a snowpack reservoir that is the primary source of streamflow for the numerous rivers originating in the Southern Rockies. The depth of snowpack is controlled by elevation and aspect, with high north-facing locations maintaining the deepest snow due to lower temperatures and reduced solar radiation. The driest season in the study area is the spring interstitial period between the end of frontal storms in April and early May and beginning of summer thunderstorms in July. Except for this dry period, no other distinct wet or dry seasons occur.

The natural distribution of *Pinus aristata* coincides with the southern half of the Southern Rockies ecoregion, extending from central and southern Colorado into northern New Mexico (Fig. 1) (Bailey, 1970). There is an additional isolated stand of *P. aristata* on the San Francisco Peaks in northern Arizona. *P. aristata* is primarily found on the xeric, south-facing aspect of mountains between 2700 and 3700 m, in locations not occupied by Engelmann spruce, subalpine fir, or aspen (Baker, 1992; Schoettle and Coop, 2017). *P. aristata* habitat coincides with the headwaters of the Rio Grande, Arkansas, and South Platte Rivers, but is rarely found west of the North American continental divide or north of 40 °N (Gilbert et al., 2019). *P. aristata* and *P. longaeva* have no range overlap, with the division largely demarcated by the Colorado River (Bailey, 1970). For this investigation we focused on the Colorado and New Mexico range of *P. aristata* (36.8 °N-39.2 °N, 105 °W-106 °W), excluding the isolated stand in Arizona.

2.2. Data

2.2.1. Tree-ring data

Ten *P. aristata* collections were used in this study — five newly sampled, four previously developed, and one an update of a previous collection (Table 1). The previously developed collections were selected from our inventory of all published and unpublished *P. aristata* ring-width data. From this inventory we selected the collections with available ring-width measurements, low incidence of dating errors (as determined by COFECHA)(Holmes, 1983), and end dates of 2000 or later to maximize the timespan for the climate response analysis. This narrowed down the previous set of collections to four sites: Black Mountain (BLK) (Brunstein and Yamaguchi, 1992; Miller, 2014; Woodhouse et al., 2011), Summitville (SMV) (Routson et al., 2011), Sheep Mountain (SHM) (Woodhouse et al., 2011), and Windy Peak (WPK) (Woodhouse unpublished). One new collection in this study, Hermit Lake (HER), was an update of a previously collected chronology (LaMarche and Stockton, 1974). Ring-width data for the five previously collected sites (including the original HER time series), were obtained from the International Tree-Ring Data Bank (ITRDB) and from the unpublished collection of one of the authors. The new *P. aristata* collection sites span the length of the Sangre de Cristo Mountains from central Colorado to northern New Mexico. The five new sample collections were: Antora Peak East (APE), Little Costilla Peak - High (LCH), Little Costilla Peak - Low (LCL), North of Heart Lake (NHL), and Zapata Trail Summit (ZTS) (Fig. 1, Table 1). These sites were identified using location data from previous genetic sampling research (Schoettle and Coop, 2017), the Arizona - New Mexico Chapter of the SEINet botanical repository (Gilbert et al., 2019), and examination of Google Earth images. The ten sites range in elevation from 2900 m at LCL to 3680 m at HER. The majority of sites (n = 7) were located on south-aspect slopes, with SHM and LCH found on east-aspect slopes, and LCL sampled on a valley floor.

During the summers of 2018 and 2019, we collected *P. aristata* increment cores from the five new sites and one updated site (Table 1). We selected the oldest trees for sampling based on a set of physical characteristics that indicate extreme age (strip-bark growth, reduced crown, presence of dead pith spike) (Brunstein, 2006). At minimum, two cores were collected from each tree with an increment borer, taken at breast height (1.3 m), with at least 15 trees sampled per site. At five of the six sites (APE, HER, LCH, NHL, and ZTS) trees were sampled at or near the upper tree line limit of growth, but with care to exclude trees with krumholtz morphology that could distort climate sensitivity and reduce cross-dating capacity. The cores were mounted and prepared in accordance with standard dendrochronological procedure (Stokes and Smiley, 1968), the cross-dated ring-widths were measured with a Velmex measuring stage to a precision of 0.001 mm, and the measurement data was stored using the Tellervo archiving software (Brewer, 2014). The years assigned to each ring-width measurement were verified with the COFECHA software (Holmes, 1983).

Because the new samples in this study were from living trees, we made an effort to select only living trees from the previous collections. In cases where the sample type was unclear, we relied on the sample code if it indicated a remnant or a living tree. All ring-width measurements

Table 1
The 10 *Pinus aristata* tree-ring collections used in this study. Site names and the site code abbreviations used in the manuscript are listed below, along with the elevation and geographic coordinates for the sampling locations. Total samples collected (i.e., cores taken with increment corer) and the number of trees sampled at each location are also included.

Site Name	Site Code	Elev.	Longitude	Latitude	Samples Collected	# of Trees Sampled	Chronology Time Period (SSS > 0.80)	Mean Tree Age
New collections								
Antora Peak East	APE	3600m	−106.200	38.327	44	20	1513–2017	423
Little Costilla Peak High	LCH	3600m	−105.243	36.784	54	21	1700–2017	249
Little Costilla Peak Low	LCL	2900m	−105.223	36.823	40	19	1826–2017	193
North of Heart Lake	NHL	3550m	−105.450	36.792	40	16	1313–2017	553
Zapata Trail Summit	ZTS	3600m	−105.486	37.647	45	17	1726–2017	214
Update of previous collection								
Hermit Lake	HER	3680m	−105.642	38.096	59	36	1394–2017	419
Previous collections								
Black Mountain	BLK	3350m	−105.689	38.713	31	17	848–2012	901
Sheep Mountain	SHM	3475m	−106.103	39.201	37	19	1495–2007	526
Summitville	SMV	3500m	−106.632	37.438	13	12	1111–2009	718
Windy Mountain (Peak)	WPK	3650m	−106.408	37.478	18	11	1136–2007	501
Collection Totals					**381**	**188**		

from these screened collections were then stored in the Tellervo database. Total number of ring-width samples and number of trees sampled for the sets of collections, along with mean age and chronology length, are shown in Table 1.

2.2.2. Climate data

PRISM monthly gridded climate data (Daly et al., 1994) were used for correlation analysis, taking advantage of the spatial extent and long period of record of the PRISM dataset. The algorithm for the gridded PRISM data includes adjustments for orographic effects on temperature and precipitation, taking into account elevation, slope, and aspect to simulate topographically induced variability (Daly et al., 1994). PRISM monthly total precipitation, monthly average maximum temperature, and monthly average minimum temperature from the period 1895–2018 were downloaded at the 0.25° resolution from the KNMI Climate Explorer (Trouet and Van Oldenborgh, 2013). The PRISM data were cropped to an area extending from 30 °N to 46 °N to 114 °W to 98 °W, centered on the study area, for use in correlation analysis (Fig. 1, climate response region).

2.3. Methods

2.3.1. Tree-ring time series development

Our goal was to investigate the potential for multiple signals both between and within collection sites, therefore we developed two separate tree-ring datasets. The first dataset ("CHRON") was a set of chronologies from each of the ten sites used to investigate growth patterns between sampling sites. The second dataset ("TREE") was a collection of 88 individual tree-ring series used for analysis of common tree-growth patterns between trees irrespective of the sampling location. Prior to developing the two datasets, we processed the data and removed juvenile growth. If multiple core samples were collected from the same tree, we averaged together the ring-width values to produce a single time series for each tree (n = 188) (Table 1). To remove juvenile growth, we identified the maximum common interval between all ten sites (1826–2007). We removed any ring-width series with evident juvenile growth over this period, resulting in the removal of ten ring-width series. We used the remaining 178 ring-width series to construct the CHRON and TREE datasets.

The ten chronologies in the CHRON dataset were developed as follows: We evaluated subsample signal strength (SSS) prior to chronology construction to identify the periods of time with a sufficient number of tree-ring width measurements to produce a strong common signal for each chronology (Buras, 2017). A cutoff value of 0.80 for SSS was used to determine which time periods to select from each chronology (Wigley et al., 1984). This produced a common interval between the ten chronologies of 1826–2007 (n = 182 years). The ring-width series for each site were truncated to match this period and standardized using the series mean. The standardized ring-width series were then combined into a chronology using the robust bi-weight mean in the R package dplR (Bunn, 2008; Cook et al., 1990). Mean-value standardization was used as it preserves potential low-frequency signals present in the measurements (Kipfmueller and Salzer, 2010). More complex detrending methods were not used for two reasons. First, almost all series used represented the last two centuries of growth in very slow-growing, long-lived trees. The few samples with possible juvenile growth during the period of chronology construction were deleted, removing the need to account for the influence of age on ring-width. Second, *P. aristata* grows in open stands in remote, undisturbed locations and has never been commercially harvested; with little to no exogenous disturbance, any low-frequency variability is assumed to be related to climate, and of interest to this study. The consistently slow growth, lack of exponential growth curve and tree-level decadal variability that merit this detrending approach are illustrated in Figure S1 in the supplemental materials.

The TREE dataset was developed as follows: We started with the 178 individual trees used to construct the CHRON dataset. Next, we screened for the trees with continuous data over the same time period as the CHRON dataset (1826–2007). A total of 88 time series met these criteria and were selected for use in the TREE dataset. They were truncated to the common interval of 1895–2007 and detrended by their mean-value to standardize the dataset prior to analysis. The number of trees per sampling site varied from three at HER to 16 at APE.

2.3.2. Determining dominant modes of tree-growth variability with EOF analysis

EOF analysis was used to isolate the dominant patterns of variability in the CHRON and TREE time series datasets, and then to evaluate which sites or set of trees contributed to the primary patterns of variability. The R program "prcomp" ran EOF analysis using SVD (singular value decomposition). A covariance matrix of the tree-ring data was used in the EOF calculation because all tree-ring data were measured in equivalent units and the mean-value detrending applied to the time series reduced the potential for a single series with excess variance to dominate the EOF results (Overland and Preisendorfer, 1982). Running an EOF

analysis decomposes the covariance matrix into eigenvectors and their corresponding eigenvalues. The eigenvectors (also called "loadings") are orthogonal (uncorrelated) and can be multiplied with the original dataset to produce a set of time series (Anchukaitis and Tierney, 2013). Each of the time series (or "scores") corresponds to a mode of variance, which, in this study, represents a particular pattern of tree growth over time. However, the forced orthogonality of the eigenvectors produced results that may not correspond with physical realities (Richman, 1986). To improve the interpretability of the loadings, a rotation procedure was applied to the EOF modes.

Before applying rotation to the original EOF modes, we determined the significant number of eigenvalues to retain using a modified N-rule calculation (Anchukaitis and Tierney, 2013; Preisendorfer and Mobley, 1988). This process utilizes a Monte Carlo approach, creating 10000 synthetic white noise (Gaussian) and red noise (lag-1 autocorrelation) datasets, applying EOF analysis to the synthetic data, then determining if the original EOF eigenvalues were greater in value than the 95th percentile of the synthetic data eigenvalues. If the original EOF eigenvalues are larger than the both the white and red noise data, they are retained. A varimax orthogonal rotation was then applied to the retained original EOF eigenvalues. This process produced the rotated EOF scores for the CHRON dataset, values we used in the climate response analysis.

We ran a modified form of EOF analysis on the TREE dataset to counter the influence of an uneven sample size between collection sites (varying from three to 16 trees). First, we applied the EOF analysis to the individual tree-growth series at each site (ten runs, one per site). The modified N-rule was used to determine the number of EOF modes from each collection site to retain (Table 3). The retained EOF modes were converted into unrotated EOF scores. EOF analysis was applied a second time to the set of unrotated EOF scores producing a final set of EOF modes. A varimax orthogonal rotation was applied to the second set of EOF modes producing rotated EOF scores. This second set of TREE EOF scores was used in our climate response analysis. The two-step process reduced the influence of sample number by converting the ring-width data into the dominant modes of growth at each site. Whereas the CHRON EOF process highlighted a single growth signal per site (i.e., chronology), the TREE EOF process allowed sites with multiple growth signals to have both growth patterns represented in the EOF analysis.

2.3.3. Determining modes of variability based on tree-growth response to climate

We utilized a second process to identify unique modes of tree-growth variability at the tree level based on methods used in a previous study of five needle pines (Kipfmueller and Salzer, 2010). Following their approach, we first investigated the correlation between local climate and each tree-growth time series, then we grouped the trees based on the types of correlations to produce clusters with similar climate responses. We then combined the tree-growth series in each cluster to produce a single tree-ring time series corresponding to the climate response of each tree cluster. This time series was used to evaluate the climate response in the same manner as the EOF scores. We refer to this as the "Tree-Climate Method."

In this approach, we took the same set of 178 tree-ring time series used to produce the CHRON and TREE datasets and selected all trees with a complete period of record from 1895–2007 (a total of 119 trees). We chose the 1895 start date to match the period of record for PRISM data. We truncated the remaining 119 series to the 1895–2007 period and detrended by their mean-value as done with the CHRON and TREE datasets. Next, we extracted the PRISM monthly precipitation, minimum temperature, and maximum temperature values for the data pixel located over each chronology location. The monthly climate data were averaged into three-month seasonal time series (previous-Fall, Winter, Spring, Summer, and Fall) in the same manner as Kipfmueller and Salzer (2010), but with additional previous-Spring and previous-Summer seasons. Each tree was correlated with the seasonal climate record at the sampling location and the resulting correlations were combined into a matrix of correlations. If a tree had no significant correlations with any climate parameter, it was dropped from the matrix, reducing the final number of trees used for the cluster analysis. The final Tree-Climate dataset used for cluster analysis consisted of 114 trees. We calculated the clusters from the matrix using hierarchical cluster analysis with Euclidean distance matrices and Ward's method (Ward, 1963). The stability of the clusters was determined with bootstrapped Jaccard indices calculated by the R function "clusterboot" (Hennig, 2007). The number of clusters to keep was determined iteratively until the average of all the Jaccard indices was highest. Once a stable number of clusters was determined, the tree-ring series within each cluster were combined using a biweight robust mean to produce a single time series (Cook et al., 1990).

2.3.4. Tree-growth/Climate analysis

We assessed the relationship between the tree-growth time series (from both chronology-level and tree-level analyses) and the PRISM gridded climate data with Pearson correlation analysis (significance assessed at $p < 0.05$). Correlations were calculated for each climate parameter (precipitation, maximum temperature, minimum temperature) and tree-growth time series, from the April of the previous year to the end of current year growing season in September ($n = 18$ months). The correlations for months in the year prior to the growing season were evaluated because of the high lag-1 autocorrelation present in *P. aristata* (LaMarche and Stockton, 1974), which may result in a growth response to climate variation in the years after the initial climate perturbation. All correlations were calculated for the time period 1895–2007 as this is the common time-period between the PRISM data and all CHRON EOF, TREE EOF, and Tree-Climate time series. Because the sign of EOF eigenvectors is arbitrary, and to facilitate comparisons, we reversed the sign of one EOF time series prior to the correlation calculations. The score for this time series had a strong negative correlation with the three Tree-Climate time series, which are representative of the original direction of the tree response to climate. Therefore, it was reversed to match the directionality of the Tree-Climate time series.

Because of the large number of correlations being run between tree-growth time series and the climate records, a high potential for spurious false positive correlations (type I errors) between the proxy record and climate data exists (Hu et al., 2017). To adjust for the high test multiplicity and concurrent increase in type 1 errors, the False Discover Rate (FDR) procedure was applied (Benjamini and Hochberg, 1995). We ran FDR using the "p.adjust" function in R with a q-value set to 0.05, the same as our p-value threshold. In addition to the corrections for high test multiplicity, adjustments were made to account for serial correlation (i.e. autocorrelation) (Hu et al., 2017). To correct for high serial correlation an adjustment equation as defined by Dawdy and Matalas (1964) was used to calculate effective degrees of freedom υ_{eff}. This adjustment increases the corresponding p-value in proportion to the increase in autocorrelation, reducing the potential for a type I errors. The FDR and υ_{eff} adjustments were applied to all calculations used in the climate response correlations, while only the υ_{eff} adjustment was applied to the seasonal climate relationships used in the Tree-Climate Method. FDR was unsuited for the initial Tree-Climate Method step as the correlations were single instance (one tree-ring time series and one climate time series), therefore reducing the need to assess potential false positives.

The climate response calculations were run a second time with the low-frequency variability removed prior to correlation. We applied a 30-year Butterworth high-pass filter to both the climate time series and the tree-growth time series using the pass.filt function in the R package DplR (Bunn, 2008). Removing the low-frequency variability allows for comparison of the high-frequency variances in the resulting time series. The loss in correlation strength following the application of a high-pass filter will highlight time series where the low-frequency variability was an important factor in correlation. Both the original and high-pass filtered correlation calculations were used to analyze the climate sensitivity of

the tree-growth time series.

From the climate response calculations, we produced a regional correlation map (Fig. 1, climate response region) for each combination of climate parameter, month, tree-growth time series, and for both the original and high-pass filtered series. These maps provide a broad overview of climate response for each time series. Next, we extracted the correlation values from a smaller region located directly over the *P. aristata* sampling sites (36 °N- 40 °N by 108 °W- 104 °W) (Fig. 1, reduced climate response region). From this reduced region, we produced a jitter plot of all correlations for the CHRON and TREE EOF time series and the Tree-Climate time series. These plots show the correlation (for $p < 0.05$) of each tree-growth time series with each monthly climate variable. They also show the variation in correlation strength whether the data was filtered or not prior to correlation. This smaller subset was used to better represent the local climate.

3. Results

3.1. Time series produced from tree-growth patterns and tree-growth climate signals

The EOF analysis based on the ten chronologies resulted in two primary modes of variability (Table 2). The first CHRON EOF (C-1), accounting for 52 % of the total variance, is composed primarily of loadings from LCH, ZTS, NHL, APE, WPK, and HER. These six sites are all located at the upper tree line. The second CHRON EOF (C-2), accounting for 23 % of the total variance, is characterized by the two lower elevation sites, BLK and LCL, and one upper elevation site, WPK. Two sites, SHM, and SMV, contribute to both EOF modes, with small positive loadings for each mode.

The first step of the TREE EOF analysis, on tree-growth series within each of the 10 sites, yielded either one or two EOFs per site (Table 3). Seven sites had only one dominant EOF mode of growth, and three sites, BLK, SHM, and SMV had two significant EOF modes within the collection site. These EOFs, 13 in all, were then used in the second round of TREE EOF analysis. This yielded two statistically significant TREE EOF modes (T-1 and T-2) representing 41 % and 21 % of the explained variance, respectively (Table 4).

The first TREE EOF mode (T-1) was characterized by very high loadings from eight EOF time series, including most of the higher elevation sites. The second TREE EOF mode (T-2) had high loadings from five of the series, including the two lowest elevations sites and WPK. These loadings are similar to those in the CHRON EOF results, but the difference is found at the three sites with two EOF modes each which were split between T-1 and T-2. The weakness of the SHM and SMV CHRON loadings contrasts with the strong loadings of SHM-1 and SMV-1 into T-2 and SHM-2 and SMV-2 into T-1. This suggests that a single chronology at these sites inadvertently blends two contrasting growth signals producing a weaker overall growth signal.

The third approach for examining tree-growth patterns (Tree-Climate or TC) was based on cluster analysis of 114 trees from the ten sampling sites and their responses to local climate grid points. This analysis resulted in five groupings (TC-1, TC-2, TC-3, TC-4, and TC-5) with respective Jaccard indices of 0.73, 0.86, 0.48, 0.48, and 0.77. Because Jaccard indices below 0.6 are unstable and do not indicate significant patterns (Hennig, 2007), we removed TC-3 and TC-4 (and the 37 trees associated with them). TC-1 consisted of trees from nine of the ten sampling sites, particularly NHL, ZTS, and LCH. TC-2 was dominated by trees at BLK, while TC-5 was made up of trees from six of the ten sampling sites (Table 5). BLK was the only site in which all samples fell into one cluster.

The associations between the seven tree-growth series (two CHRON EOFs, two TREE EOFS, three Tree-Climate clusters) were examined for the common period, 1895–2007 (Fig. 2). The EOF time series pairs (C-1/C-2 and T-1/T-2) had weak correlations with one another, a logical

Table 2
The CHRON EOF loadings from each sampling site for EOF's C-1 and C-2.

Site Code	C-1 EOF Loadings	C-2 EOF Loadings
APE	0.232	0.015
BLK	−0.022	0.248
HER	0.208	0.012
LCH	0.313	−0.021
LCL	−0.050	0.254
NHL	0.238	0.061
SHM	0.051	0.060
SMV	0.082	0.153
WPK	0.217	0.225
ZTS	0.280	0.041
Explained Variance	**52.44%**	**23.41%**

Table 3
The number of trees per sampling site used in first EOF analysis and the number of significant EOF modes retained per sampling site for use in Step 2 of the TREE EOF analysis. The explained variance for each site's EOF mode is also included.

Site Code	# of Trees	# of Significant EOF Modes	Explained Variance EOF-1	Explained Variance EOF-2
APE	16	1	58.60%	–
BLK	14	2	58.14%	12.74 %
HER	3	1	55.70%	–
LCH	10	1	64.51%	–
LCL	4	1	69.66%	–
NHL	12	1	57.80%	–
SHM	8	2	40.55%	23.55 %
SMV	10	2	50.65%	14.59 %
WPK	5	1	66.72%	–
ZTS	6	1	53.26%	–
Total	**88**	**13**		

Table 4
The loadings for TREE EOF time series T-1 and T-2, using the EOF Scores from TREE EOF Step 1 (see Table 3).

Step 1 TREE EOF Time Series	T-1 EOF Loadings	T-2 EOF Loadings
APE	0.902	0.004
BLK-1	0.014	0.862
BLK-2	0.827	−0.142
HER	0.384	0.220
LCH	0.928	−0.100
LCL	−0.175	0.802
NHL	0.841	0.269
SHM-1	−0.110	0.735
SHM-2	0.671	−0.094
SMV-1	0.264	0.618
SMV-2	0.689	−0.081
WPK	0.573	0.540
ZTS	0.844	0.233
Explained Variance	**41.27%**	**21.11%**

Table 5
The number of trees used in each Tree-Climate cluster shown by sampling site. The number of total trees per side does not match the number of trees used because TC-3 and TC-4 were dropped from the analysis prior to correlation with climate.

Site Code	Total # of Trees	# of Trees Used	TC-1	TC-2	TC-5
APE	16	8	3	5	0
BLK	15	12	0	12	0
HER	5	5	3	0	2
LCH	14	11	7	0	4
LCL	9	5	2	3	0
NHL	15	12	9	0	3
SHM	8	7	3	2	2
SMV	10	3	2	1	0
WPK	7	2	1	0	1
ZTS	15	12	8	2	2
Total Trees	**114**	**77**	**38**	**25**	**14**

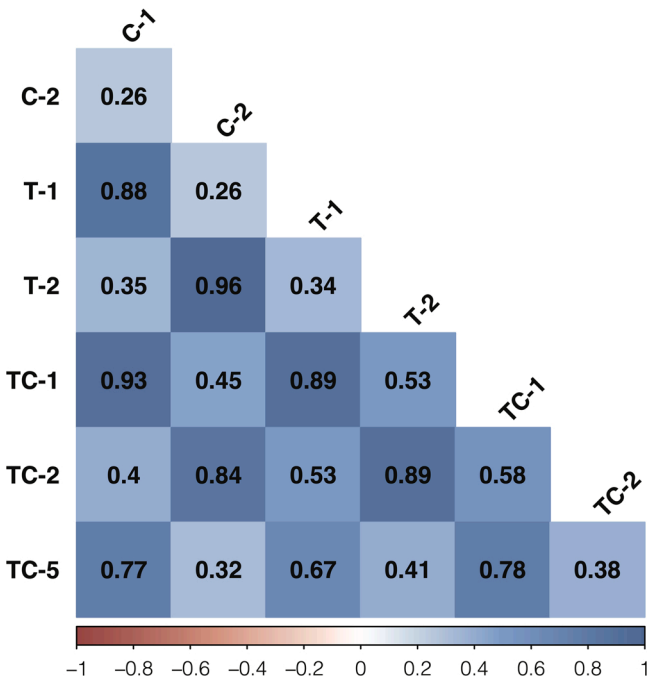

Fig. 2. Correlation matrix between all seven time series used in analysis. Pearson correlation with a threshold value of 0.05 for analysis. Each correlation is for the common period of all seven time series (1895-2007).

result as EOF modes should be orthogonal and uncorrelated. The residual correlations that do exist between EOF time series pairs are a result of the shortened period for correlation (1895–2007) relative to the full time period for the EOF analysis (1826–2007). There are broad similarities between the pairs of TREE EOFs and CHRON EOFs even though the TREE EOF is an effort to optimize the common signal by identifying within-site growth signals. For example, C-1 has a very high correlation with T-1 (0.88), while C-2 has a very high correlation with T-2 (0.96), producing two groups of time series with similar variability. The strong correlation between the two EOF pairs increases the utility of having the Tree-Climate method as an alternate mode of tree-growth analysis. The Tree-Climate time series TC-1 and TC-5 correlate strongly with the first group (C-1/T-1), while TC-2 correlates with the second group (C-2/T-2). However, these correlations are not as strong as the intra-EOF correlations. The TC time series were also all significantly correlated with one another, but TC-1 and TC-5 had the strongest correlation of 0.78.

3.2. Climate response

Climate response results indicate two main types of tree-growth/climate relationships consistent among the three sets of tree-growth patterns analyses. The first relationship, found in all seven time series, shows a negative June maximum temperature response. Six of these seven series (all but T-1) also show a positive June precipitation response. The second, and less common, climate response relationship was a positive correlation with minimum temperature during August and September at three sites (C-1, T-1, and TC-1). In the following sections we will discuss the two climate response patterns in more detail, including the influence of the high-pass filter on these relationships and the associated spatial patterns.

3.2.1. June correlations

Five of the seven time series show a significant correlation with both June precipitation and maximum temperature (C-2, T-2, TC-1, TC-2, and TC-5) (Figs. 3 and 4) in the original and high-pass filtered series, suggesting a robust June drought stress response to warm, dry conditions in that month. One additional series (C-1) is correlated with June precipitation, but does not show any correlation with June maximum temperature prior to high-pass filtering, and one (T-1) is not correlated June precipitation or with June maximum temperature prior to high-pass filtering. The removal of low-frequency variability in the C-1 and T-1 time series exposes an underlying high-frequency negative response to June temperature in these growth series (Figs. 3 and 4).

T-2 has the strongest single negative correlation with June maximum temperature ($r = -0.62$), and the strongest single positive correlation with June precipitation ($r = 0.47$) (Fig. 5A and Fig. 5C, respectively), with weaker but still significant correlations after the 30-yr high-pass filtering (Fig. 5B and Fig. 5D, respectively). The C-2 series prior to high-pass filtering also has very strong negative June maximum temperature and positive June precipitation correlations of $r = -0.58$ and $r = 0.44$ respectively. Several of the tree-growth series show positive precipitation/negative maximum temperature responses with other months; however, none of these correlations are found consistently across all seven series. Negative maximum temperature correlations during the July of the previous year are the most prevalent of these, occurring with original correlations in three of the seven time series, and with six of the seven time series after the high-pass filter is applied.

The spatial patterns of the June temperature correlations are similar for the seven tree-growth series, especially after application of the high-pass filter (Fig. 6). The highest correlations are all centered directly over the study region, weakening with radial distance from this region. Tree-growth associations with June precipitation are somewhat more variable. All but T-1 show correlations with the high-pass filtered tree-growth series that extend in a north-south pattern coinciding with the Rocky Mountains; however, the location of strongest precipitation correlation varies between the series (Fig. 7). The strongest June precipitation correlation is centered over the study area in the C-2, T-2, and TC-2 series, while it is centered over the northern Rocky Mountains in C-1, TC-1, and TC-5. The position of highest correlation is more stable with the June maximum temperature correlations and shifts in spatial correlation do not occur to the same degree as the precipitation climate correlations.

3.2.2. Minimum temperature correlations

The second main tree-growth/climate pattern is an association between tree growth and minimum temperatures. Three time series (C-1, T-1, and TC-1) feature significant positive correlations with minimum temperatures during the months of August and September, prior to application of the 30-yr high pass filter (Figs. 3 and 4). Two of these also have weak June moisture stress signals. The application of the high-pass filter removes any significant minimum temperature correlations in all three series. This is evident in the correlation maps for August and September shown for T-1 (Fig. 8). The original (un-filtered) T-1 has the strongest correlation with minimum temperature in August and September, with maximum r-values of 0.49 and 0.45 respectively, but after application of the 30-year high-pass filter the correlation map shows no significant correlations remain. The original series show a concurrent increase in both August minimum temperatures and tree-ring widths over the 20th century (Fig. 5E). Once the high-pass filter is applied (Fig. 5F), the trend is removed, and the correlation drops to 0.22, with a significance level of $p = 0.010$ after FDR and v_{eff} adjustments are applied.

4. Discussion

The analyses described here are the first undertaken to investigate the climate information in *P. aristata* tree growth across much of its range. The tree-growth/climate patterns are complex, similar to the results found by Bunn et al. (2018) for *Pinus longaeva* in the Great Basin. As with *P. longaeva*, the results from our study indicate that different growth responses occur within a single site, and in certain cases these responses indicate differing climate responses.

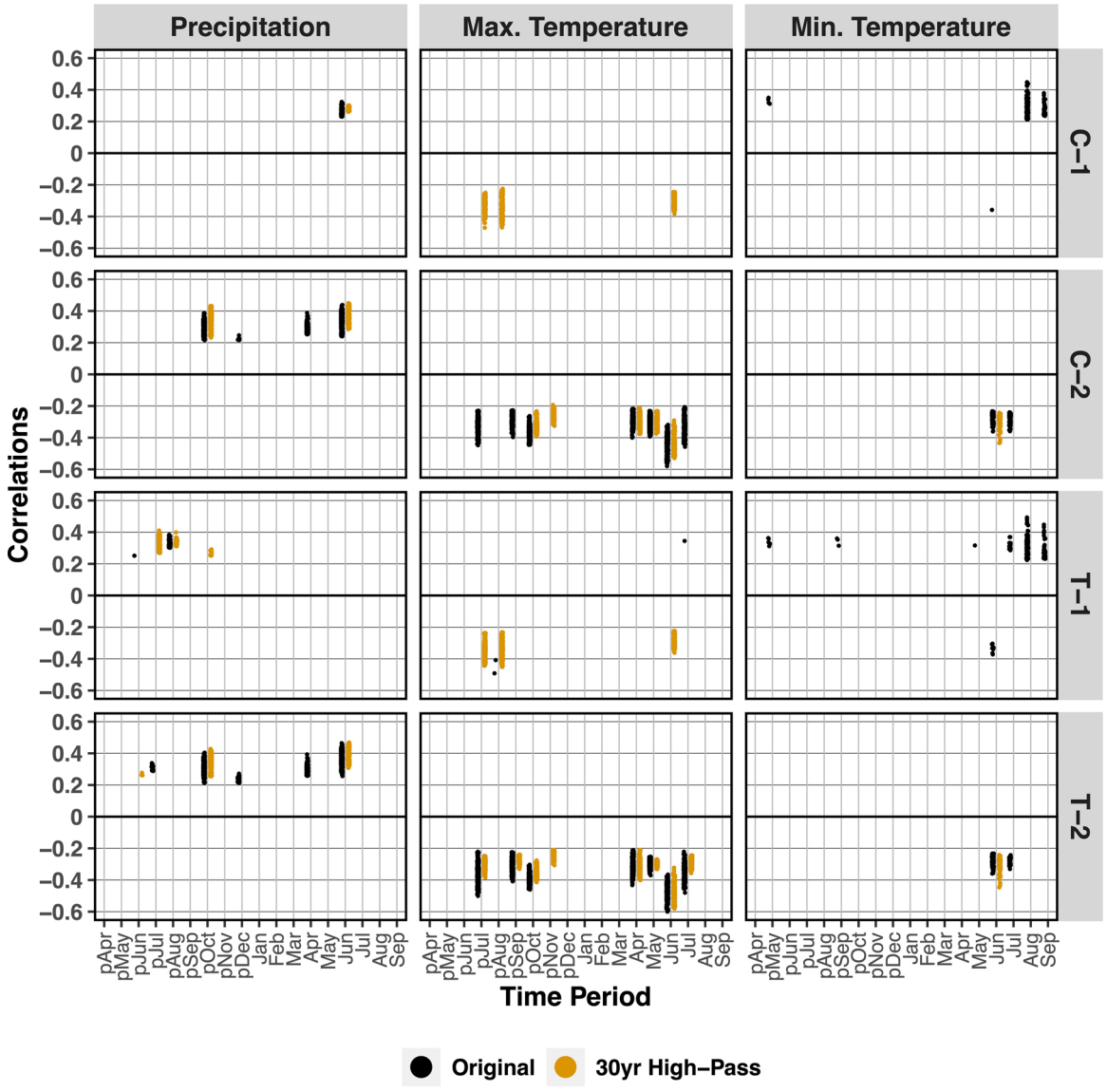

Fig. 3. Climate responses for the CHRON EOF and TREE EOF tree-growth time series. Correlation map results are compressed into jitter plots. Each cluster of points shows the range of Pearson correlations ($p < 0.05$) for each tree-growth series and monthly precipitation and temperature, from April prior to the growth year to September of the growth year. Correlations for the original (no filter) series are shown in black and for the 30-yr high-pass series in orange.

Our first research question asked whether common tree-growth signals were found between the ten *P. aristata* chronologies, and if so, how those signals related to climate variability. The CHRON EOF analysis yielded two time series (C-1 and C-2), together accounting for 76 % of the common variance among the ten chronologies. This result indicates two common tree-growth signals, one for trees at higher elevations (C-1) and one for trees at lower elevations (C-2). The C-1 series primarily shows a positive association with late summer minimum temperature while C-2 displays a strong moisture stress signal (positive correlation with precipitation and negative with temperature) that is particularly strong for June. However, when stripped of low-frequency signals using the 30-yr high-pass filter, both modes share a June drought stress response. This indicates that while upper elevation trees are showing a positive low-frequency response to late summer minimum temperatures, when examined on a more annual basis, they display a response to June drought conditions that is similar to the lower elevation *P. aristata*. Spatial patterns of correlations indicate some differences in the June drought stress signal, with the strongest June precipitation correlation centered over Wyoming for C-1 and over central Colorado, and more widespread for C-2 (Fig. 7). The maximum temperature correlation patterns are more similar to one another then the drought stress signal (Fig. 6).

Our second question asked whether multiple climate responses may exist among trees within a single *P. aristata* sampling site. This question addressed the issue of trees within the same chronology having different responses to climate due to microsite conditions. Two approaches were taken to investigate this potential problem. First, EOF analysis was performed on the individual tree-ring width series at each of the ten collection sites, followed by an EOF analysis on the modes produced for each site. Second, cluster analysis was performed on the pattern of tree-growth/climate correlations for each tree.

In the first case, an analysis of the two TREE EOF time series (T-1 and T-2) indicated a mix of growth signals within several of the *P. aristata* sampling sites. The BLK, SHM, and SMV sampling sites had two significant EOF modes after the first run of TREE EOF analysis (Table 3). The two modes from each site fell into either T-1 or T-2 when the second EOF analysis was applied (Table 4). BLK-1, SHM-1, and SMV-1 had high loadings in T-2 while BLK-2, SHM-2, and SMV-2 had high loadings in T-1. The growth patterns of the trees within these three sites are different enough to fall into two modes and remain separate in the subsequent

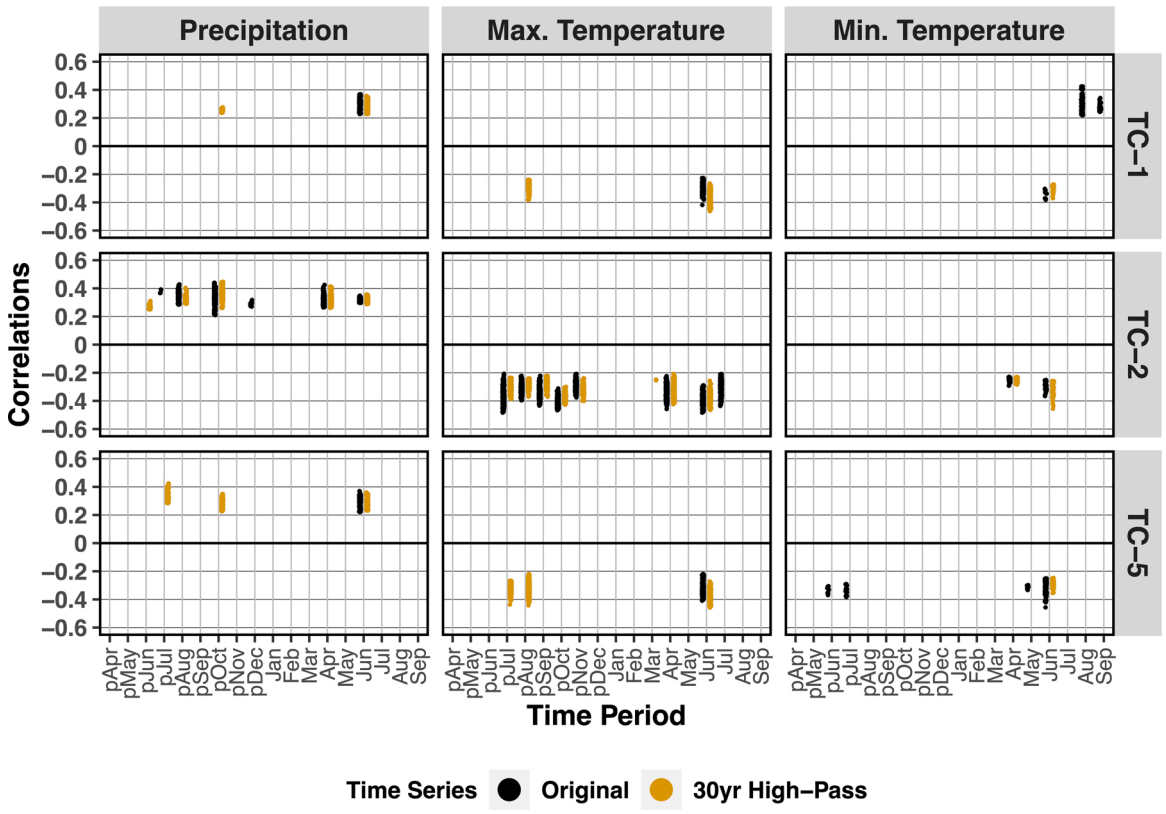

Fig. 4. Climate responses for the Tree-Climate tree-growth time series. Correlation map results are compressed into jitter plots. Each cluster of points shows the range of Pearson correlations ($p < 0.05$) for each tree-growth series and monthly precipitation and temperature, from April prior to the growth year to September of the growth year. Correlations for the original (no filter) series are shown in black and for the 30-yr high-pass series in orange.

EOF analysis. If growth pattern differences are primarily related to climate, we would expect the correlations between climate and the two TREE time series to reflect the differences. This was the case, with T-1 containing a positive, late summer correlation with minimum temperature and T-2 showing a strong June drought stress signal. These results were very similar to C-1 and C-2, respectively, with the same loss of the minimum temperature correlation for T-1 after high-pass filtering and replacement with a negative association with June (and prior summer) maximum temperature. However, the separation of different signals at BLK, SHM, and SMV sites appears to have strengthened the signal of the T-2 time series producing higher correlations with June precipitation and maximum temperature than occurs in C-2. This may indicate the mixed signals present at the BLK, SHM, and SMV sites reduced the clarity of the growth signal of their respective chronologies and subsequently of the CHRON EOF time series.

The Tree-Climate cluster analysis further suggests the potential for trees to have differing climate responses within the same sampling site. The three significant Tree-Climate clusters indicate three different tree-growth responses may be present within a single sampling site. Two sites (SHM and ZTS) have trees in all three clusters, one site (BLK) has trees in a single cluster, and the remaining seven sites have trees in two of the clusters. The presence of multiple growth patterns again represents the presence of multiple climate responses. TC-1 contains a weak late summer positive minimum temperature signal similar to C-1 and T-1, while TC-2 and TC-5 exhibited a June precipitation and maximum temperature correlation similar to C-2 and T-2. Like the previous time series, the application of the 30-yr high-pass filter removed the minimum temperature signal.

An examination of the Tree-Climate clusters suggests, that in all cases (BLK being the exception), trees within a site may contain differences in climate signal that could be related to microsite conditions. These microsite differences appear to exist at both low and high elevation sampling sites. An examination of the precise location of predominantly June drought-stressed trees compared to those with low-frequency positive summer temperature response may reveal differences in microsite characteristics. The differences in climate responses among the three Tree-Climate series are subtle after the low-pass filtering, but as with the TREE EOF results, some attention to the climate signal at the tree level may help refine the climate information. These results strongly suggest that legacy *P. aristata* collections should be used with care, as they may contain trees with a mix of climate signals.

4.1. Physical mechanisms for climate responses

The predominant June precipitation/maximum temperature correlation with tree growth we observed makes sense considering the regional climatology, the timing of tree growth, and tree physiology. First it should be noted that June is the driest or second driest month at all of sampling sites. June falls between the period of active mid-latitude winter storms and the onset of mid-summer moisture in July (Sheppard et al., 2002). June precipitation is also inversely correlated with June maximum temperature across the study region (Daly et al., 1994). While there are no published studies of cambial phenology, or the timing of wood formation, for *P. aristata*, they do exist for *P. longaeva* (Ziaco et al., 2016). *P. longaeva* is the closest genetic relative of *P. aristata* (Montes et al., 2019), therefore they likely share similar physiological traits. Analysis of cambial phenology of high altitude (3300 m) *P. longaeva* indicates xylogenesis (or onset of xylem cell formation) begins in early June and is continuous until late August at which point the annual tree-ring width is completed (Ziaco et al., 2016). The onset of xylogenesis in *P. longaeva* is driven by an interaction between soil temperature and soil moisture content. Winter snowmelt provides the moisture for *P. longaeva* xylogenesis, but the requirement of sufficient cambial warming shifts the onset of tree growth to June when the soil moisture

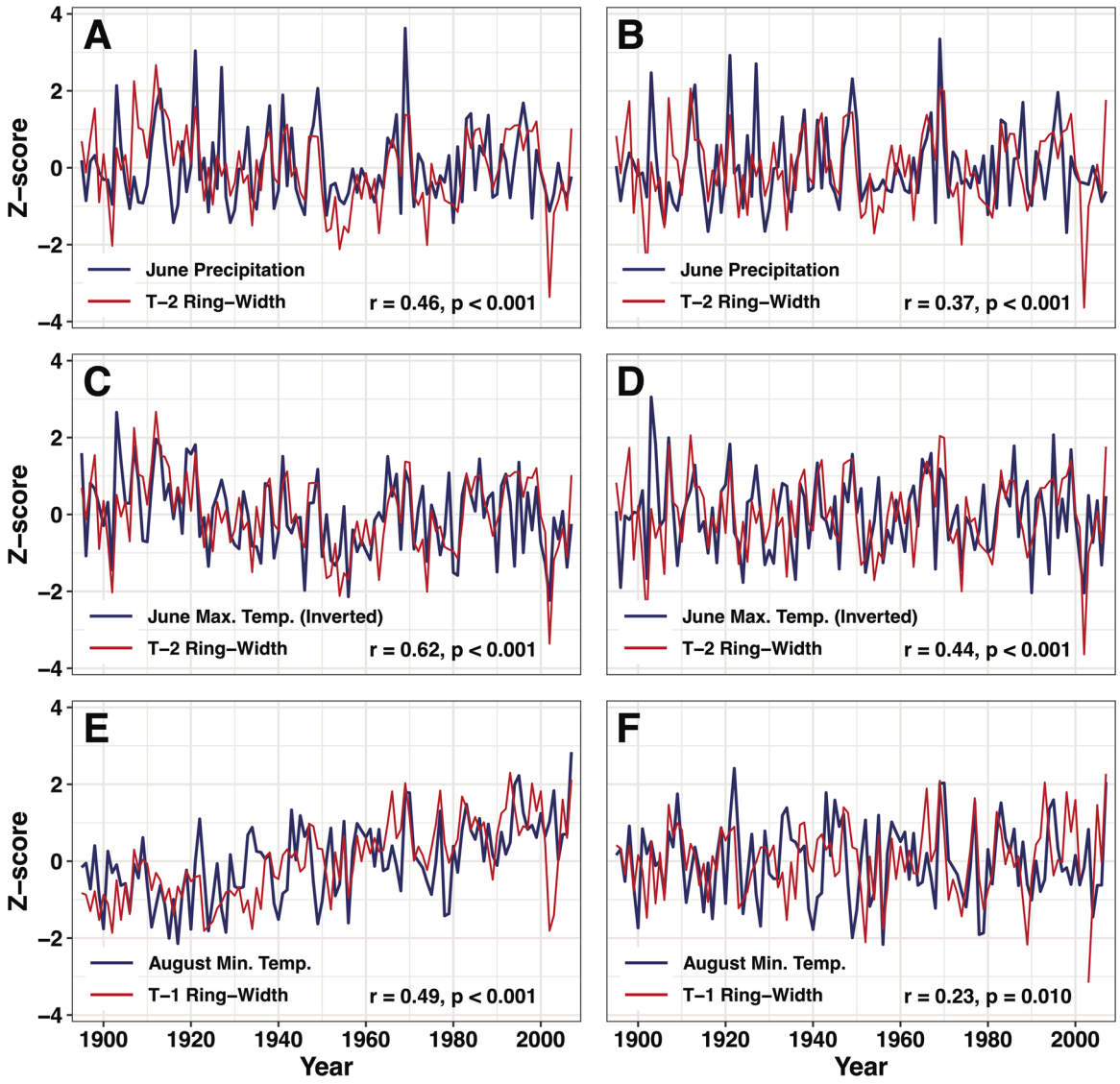

Fig. 5. Best fitting tree-growth and climate unfiltered time series (A, C, E) and the subsequent results after 30-yr high-pass filtering is applied (B, D, F) over the period 1895-2007. Climate data includes June precipitation (A, B), June maximum temperature (C, D), and August minimum temperature (E, F). Time series T-2 is used in subplots A, B, C and D, while time series T-1 is used in subplots E and F. All climate data (blue) and tree-growth data (red) are standardized to facilitate comparison. June maximum temperature data (C/D) are inverted due to the negative correlation between maximum temperature and tree growth. Correlation r-values and adjusted p-values for each subplot are included (for interpretation of the references to colour in this figure legend, the reader is referred to the web version of this article).

derived from the snowpack is most depleted (Ziaco et al., 2016). As *P. aristata* is also found in areas with low June precipitation, we propose that the onset of growth for *P. aristata* is also occurring during this same period of water stress. At our study sites, low precipitation and the corresponding high maximum temperatures in June could combine to increase water stress for *P. aristata* and delay the onset of xylogenesis, resulting in a narrower tree ring. Hughes and Graumlich (1996) also found a similar relationship between *P. longaeva* growth and current spring precipitation, further supporting an indication of shared tree physiology between *P. aristata* and *P. longaeva*.

Unlike the June precipitation/maximum temperature correlation, the positive correlation with minimum temperature in C-1, T-1, and TC-1 is a low-frequency signal, not evident after the high-pass filter is applied. The correlation with minimum temperature in August and September overlaps with the period where xylogenesis is ending (Ziaco et al., 2016). Upper tree line is determined primarily by temperature controls on the process of xylogenesis, with a threshold growing season average temperature controlling the position of tree line (Körner, 2012). Trees at or near the tree line, such as our T-1 samples from APE, LCH, NHL, and ZTS, exist at the threshold for sufficient growing season temperatures, with any large deviation having potentially out-sized effects on growth (Körner, 2012). Therefore, when the months of August and September have warmer than average minimum temperatures, this could provide the needed thermal energy for these trees to extend the period of cellular division and produce a wider tree-ring. Our results show a steady increase in T-1 and C-1 ring-widths after the mid 1800s (Fig. 5E), corresponding with a steady Northern Hemisphere increase in temperature seen in other tree-ring proxies (Wilson et al., 2016). The trend may also correspond with increases in annual minimum temperature observed across the semi-arid western U.S. (Sambuco et al., 2020; Tang and Arnone, 2013), and the recent rapid increase in summer minimum temperature seen in New Mexico (Frankson et al., 2019).

4.2. *Potential for climate reconstruction*

Our final question asked what the potential is for developing long

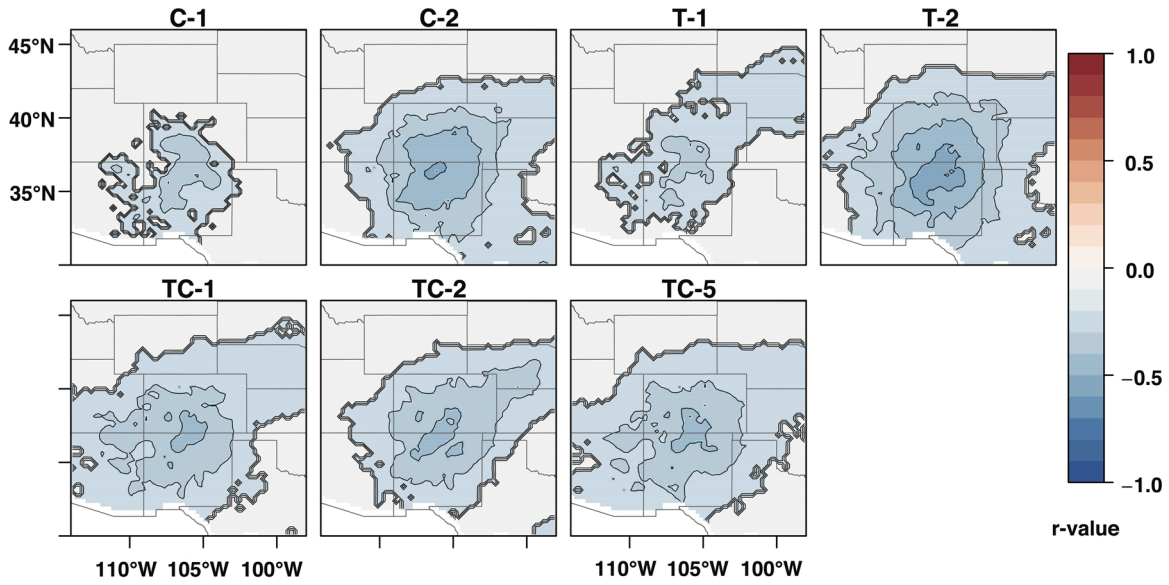

Fig. 6. June 1-month maximum temperature field correlation maps for each of the seven tree-growth series. Each coloured pixel represents a significant Pearson correlation ($p < 0.05$) between the June 1-month maximum temperature at that pixel and the tree-growth series. These maps show the results when the 30-yr high-pass filter is applied to both the climate record and tree-growth time series prior to correlation. R-values are broken into intervals of 0.1 for clarity, with map contour lines delineating the boundary between each interval.

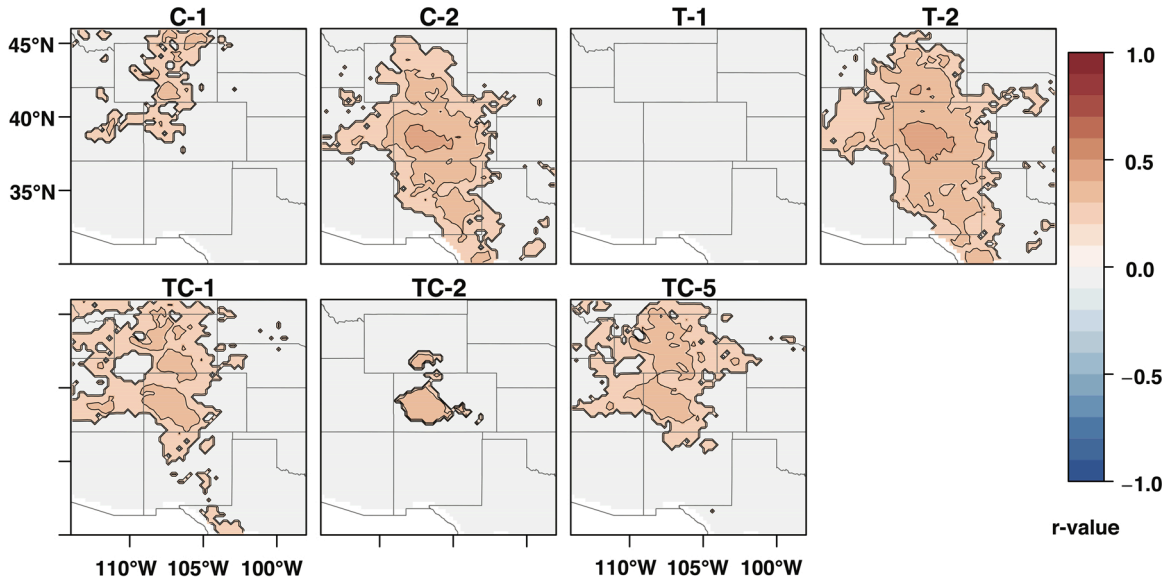

Fig. 7. June 1-month precipitation field correlation maps for each of the seven tree-growth series. Each coloured pixel represents a significant Pearson correlation ($p < 0.05$) between the June 1-month precipitation at that pixel and the tree-growth series. These maps show the results when the 30-yr high-pass filter is applied to both the climate record and time series prior to correlation. R-values are broken into intervals of 0.1 for clarity, with map contour lines delineating the boundary between each interval.

moisture and/or temperature reconstructions from this set of data. The *P. aristata* June moisture stress signal (positive precipitation/negative maximum temperature correlation) has the greatest potential for long-term reconstruction. Two flavors of signal exist across the seven sites. The first is robust, found at the low elevation sites (BLK, LCP) and those sites with multiple within-site growth patterns (SHM, SMV), and maintains its correlation with June climate after high-pass filtering. The time series plot of filtered June precipitation and tree growth suggests that some decadal-scale variability exists in the precipitation data that is reflected in the tree-ring series (Fig. 5), and this should be considered in the reconstruction process. The second flavor is weaker, found at high elevation sites, and is revealed only after the dominant minimum temperature signal is removed using high-pass filtering. Both groups could be combined to produce a single regional June moisture reconstruction; however, if the reconstruction were to include remnant samples with unknown climate correlations, caution would warrant the creation of a climate reconstruction using only the lower elevation sites where minimum temperature is not known to have a positive effect on growth.

P. aristata also shows potential for temperature reconstruction, but further research and sampling are likely required before this can be done with confidence. One issue with these trees is the strong reduction in the positive correlation with minimum temperature for C-1 and T-1 following the application of the 30-yr high-pass filtering. This may indicate the minimum temperature correlations are mostly due to similarities in low-frequency, multi-year patterns in temperature, rather than year to year variability. A similar issue was encountered during the

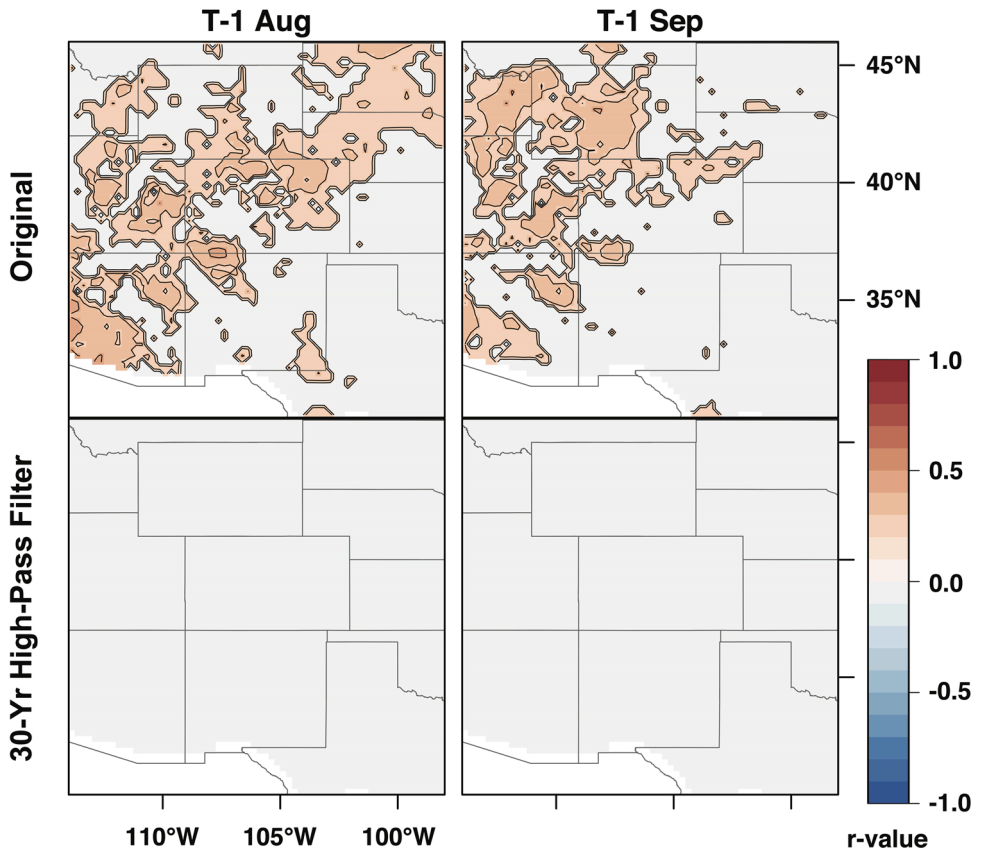

Fig. 8. August (left) and September (right) 1-month temperature field correlation maps for T-1 original (no filter) and 30-yr high-pass filtered tree-growth series. Each coloured pixel represents a significant Pearson correlation ($p < 0.05$). R-values are broken into intervals of 0.1 for clarity, with map contour lines delineating the boundary between each interval.

production of a temperature reconstruction using *P. longaeva* (Salzer et al., 2014a). In that case, a 20-year smoothing spline was used to enhance the low-frequency signals and improve the strength of the temperature correlation. A future *P. aristata* temperature reconstruction may also be improved using a similar smoothing calculation. Another issue hampering a temperature reconstruction is the question of whether remnant samples can be used with confidence to reproduce temperature. The sampling sites with temperature sensitive trees contained multiple climate response signals and the remnants at those sites may also contain a similar mix of climate signals. One prospective solution could be a demographic study of a sampling site with intensive sampling that accurately maps the distribution and cohorts of trees over multiple centuries. The shifting proximity of a remnant to upper tree line could potentially be used as a proxy for increased temperature sensitivity and allow incorporation into a temperature reconstruction. Another approach could couple fine scale temperature measurements across an elevational gradient at a sampling site with growth modeling to better understand the temperature thresholds that result in tree growth limited by temperature rather than moisture. Both of these approaches have been utilized with *P. longaeva* (Bruening et al., 2018, 2017; Tran et al., 2017) and could be applied to *P. aristata*.

5. Conclusions

Rocky Mountain bristlecone pine (*P. aristata*) has the potential to skillfully reconstruct June moisture variability in the Southern Rocky Mountains, with a secondary potential to reconstruct a low-frequency component of late summer minimum temperatures contingent upon additional investigatory work. Mixed climate responses within single sampling sites necessitate the careful selection of individual trees for use in climate reconstructions when using the existing chronologies. The dominant *P. aristata* tree-ring growth signal in Colorado and New Mexico is a current year June precipitation and maximum temperature sensitivity, explained by a plausible physical mechanism. The extent of this climate response across multiple sampling sites makes it an ideal parameter for a climate reconstruction. There also exists a separate set of trees with a low-frequency long-term positive response to temperature simultaneously present in trees with a weak June drought stress response at higher frequency. These temperature sensitive trees also have a potential for climate reconstruction, albeit one requiring more intensive sampling and screening for temperature response.

There are few late-spring/early-summer tree-ring precipitation reconstructions for the western U.S. outside a *P. longaeva* reconstruction in California (Hughes and Graumlich, 1996) and a Douglas fir/Limber pine reconstruction in Wyoming (Gray et al., 2004). The majority of tree-ring precipitation reconstructions are correlated with the winter prior to the current growing season. Gridded PDSI datasets such as the North American Drought Atlas (NADA) also largely reflect a cool season moisture signal (Cook et al., 2010). Streamflow in the semi-arid western U.S. peaks in late-spring/early-summer as the winter snowpack provides water through a typically dry period. Increases in late-spring/early-summer precipitation have been shown to extend the period of snowmelt runoff in high elevation river basins (Dudley et al., 2017). A *P. aristata* reconstruction could provide a record of years with a cool, wet June versus those years with a warm, dry June, adding to our pre-instrumental understanding of this relationship between winter and early summer moisture.

The original impetus for this study was the need for more tree-ring based temperature reconstructions in the semi-arid Western U.S. While our results primarily point to a June drought signal, there does exist a weaker but still significant correlation with late summer minimum temperature. Future work is needed to overcome the limitations of

this study, including the construction of chronologies with a higher number of constituent samples and a more informed approach to sampling for temperature. A next step in this work is the utilization of a process-based modeling approach (Vaganov et al., 2006; Anchukaitis et al., 2020) to better select trees for temperature sensitivity. Research on *P. aristata* cambial physiology is also needed to understand the environmental factors (including temperature) controlling ring-width growth. This could be accomplished through intensive cambial phenology (Ziaco et al., 2016). Work on tree proxies other than ring-width, such as cellular anatomy (Ziaco et al., 2016), latewood density (Briffa et al., 2001), or blue light intensity (Campbell et al., 2007) may also produce *P. aristata* time series with stronger temperature correlations.

These results represent a first step in understanding the complexity of climate sensitivity in *P. aristata*. We assumed that a close genetic relationship between with *P. longaeva* and *P. aristata* would result in complexities that are similar to those found in *P. longaeva,* and our study confirmed this assumption. Any work utilizing existing *P. aristata* chronologies must recognize this complexity and take care in sample selection to screen for the climatic response under investigation. While our focus for this investigation was on the growth patterns of living *P. aristata* trees, we were fortunate to sample a large collection of remnant wood for future work at four sampling sites (APE, HER, NHL, and ZTS). These sites contained an abundant selection of downed trees, many over 2000 years in age. At APE and NHL, we constructed continuous chronologies dating back to 847 BCE and 778 BCE respectively. To the best of our knowledge, these represent the oldest and longest dendrochronologic collection of any tree species for both Colorado and New Mexico.

Future efforts to clarify the connection between *P. aristata* tree growth and climate variability will provide the framework to develop multi-millennial tree-ring climate reconstructions from these ancient chronologies. This work could deepen our understanding of the controls on past hydroclimate interactions, improving our understanding of how natural variability underlies and interacts with climate change.

Declaration of Competing Interest

The authors have no competing interests.

Acknowledgements

Funds for this study were provided by the National Science Foundation grant (Award No. 1702271). We are grateful to Lindsay Cutler, Mark Losleben, Trevor Birt, Soumaya Belmecheri, Matthew Meko, Flavio Lehner, Angeline Pendergrass, Andy Wood, and Sean Fleming for assistance collecting samples in the field. We are particularly grateful to Kyler McNeely for his preparation and measurement of countless samples in the lab and to Jeff Lukas for his contributions to development of the Sheep Mountain, Black Mountain, and Windy Peak collections. We also thank all the contributors of the tree-ring data used in this study, and two anonymous reviewers whose comments and suggestions helped improve this paper.

Appendix A. Supplementary data

Supplementary material related to this article can be found, in the online version, at doi:https://doi.org/10.1016/j.dendro.2021.125846.

References

Anchukaitis, K.J., Tierney, J.E., 2013. Identifying coherent spatiotemporal modes in time-uncertain proxy paleoclimate records. Clim. Dyn. 41, 1291–1306.
Anchukaitis, K.J., Evans, M.N., Hughes, M.K., Vaganov, E.A., 2020. An interpreted language implementation of the Vaganov–Shashkin tree-ring proxy system model. Dendrochronologia 60, 125677.
Bailey, D.K., 1970. Phytogeography and taxonomy of Pinus subsection Balfourianae. Ann. Mo. Bot. Gard. 210–249.
Baker, W.L., 1992. Structure, disturbance, and change in the bristlecone pine forests of Colorado. U.S.A. Arct. Alp. Res. 24, 17. https://doi.org/10.2307/1551316.
Benjamini, Y., Hochberg, Y., 1995. Controlling the false discovery rate: a practical and powerful approach to multiple testing. J. R. Stat. Soc. Ser. B Methodol. 57, 289–300.
Berkelhammer, M., Stott, L., 2012. Secular temperature trends for the southern Rocky Mountains over the last five centuries. Geophys. Res. Lett. 39.
Blasing, T., Fritts, H., 1976. Reconstructing past climatic anomalies in the North Pacific and western North America from tree-ring data. Quat. Res. 6, 563–579.
Brewer, P.W., 2014. Data management in dendroarchaeology using Tellervo. Radiocarbon 56, S79–S83.
Briffa, K.R., Jones, P., Schweingruber, F., 1992. Tree-ring density reconstructions of summer temperature patterns across western North America since 1600. J. Clim. 5, 735–754.
Briffa, K.R., Osborn, T.J., Schweingruber, F.H., Harris, I.C., Jones, P.D., Shiyatov, S.G., Vaganov, E.A., 2001. Low-frequency temperature variations from a northern tree ring density network. J. Geophys. Res. Atmos. 106, 2929–2941.
Bruening, J.M., Tran, T.J., Bunn, A.G., Weiss, S.B., Salzer, M.W., 2017. Fine-scale modeling of bristlecone pine treeline position in the Great Basin. USA. Environ. Res. Lett. 12, 014008.
Bruening, J.M., Bunn, A.G., Salzer, M.W., 2018. A climate-driven tree line position model in the White Mountains of California over the past six millennia. J. Biogeogr. 45, 1067–1076.
Brunstein, F.C., 2006. Growth-Form Characteristics of Ancient Rocky Mountain Bristlecone Pines (Pinus aristata). U.S. Geological Survey, Colorado.
Brunstein, F.C., Yamaguchi, D.K., 1992. The oldest known Rocky Mountain bristlecone pines (Pinus aristata Engelm.). Arct. Alp. Res. 24, 253–256.
Bunn, A.G., 2008. A dendrochronology program library in R (dplR). Dendrochronologia 26, 115–124.
Bunn, A.G., Hughes, M.K., Salzer, M.W., 2011. Topographically modified tree-ring chronologies as a potential means to improve paleoclimate inference. Clim. Change 105, 627–634.
Bunn, A.G., Salzer, M.W., Anchukaitis, K.J., Bruening, J.M., Hughes, M.K., 2018. Spatiotemporal variability in the climate growth response of high elevation bristlecone pine in the White Mountains of California. Geophys. Res. Lett. 45, 13–312.
Buras, A., 2017. A comment on the expressed population signal. Dendrochronologia 44, 130–132.
Campbell, R., McCarroll, D., Loader, N.J., Grudd, H., Robertson, I., Jalkanen, R., 2007. Blue intensity in Pinus sylvestris tree-rings: developing a new palaeoclimate proxy. Holocene 17, 821–828.
Chavarria, S.B., Gutzler, D.S., 2018. Observed changes in climate and streamflow in the upper Rio Grande Basin. JAWRA J. Am. Water Resour. Assoc. 54, 644–659.
Cook, E., Briffa, K., Shiyatov, S., Mazepa, V., Jones, P., 1990. Data analysis. Methods of Dendrochronology. Springer, pp. 97–162.
Cook, E.R., Woodhouse, C.A., Eakin, C.M., Meko, D.M., Stahle, D.W., 2004. Long-term aridity changes in the western United States. Science 306, 1015–1018.
Cook, E.R., Seager, R., Heim Jr., R.R., Vose, R.S., Herweijer, C., Woodhouse, C., 2010. Megadroughts in North America: placing IPCC projections of hydroclimatic change in a long-term palaeoclimate context. J. Quat. Sci. 25, 48–61.
D'Arrigo, R.D., Jacoby, G.C., 1991. A 1000-year record of winter precipitation from northwestern New Mexico, USA: a reconstruction from tree-rings and its relation to El Niño and the Southern Oscillation. Holocene 1, 95–101.
Daly, C., Neilson, R.P., Phillips, D.L., 1994. A statistical-topographic model for mapping climatological precipitation over mountainous terrain. J. Appl. Meteorol. Climatol. 33, 140–158.
Dawdy, D., Matalas, N., 1964. Statistical and Probability Analysis of Hydrologic Data, Part III: Analysis of Variance, Covariance and Time Series, Handbook of Applied Hydrology: a Compendium of Water-resources Technology. McGraw-Hill.
Deser, C., Phillips, A.S., Alexander, M.A., Smoliak, B.V., 2014. Projecting North American climate over the next 50 years: uncertainty due to internal variability. J. Clim. 27, 2271–2296.
Doesken, N.J., Pielke Sr, R.A., Bliss, O.A., 2003. Climate of Colorado, Climatography of the United States No. 60. Colorado Climate Center, Atmospheric Science Department. Colorado State University, Fort Collins, CO.
Dudley, R.W., Hodgkins, G.A., McHale, M., Kolian, M.J., Renard, B., 2017. Trends in snowmelt-related streamflow timing in the conterminous United States. J. Hydrol. (Amst) 547, 208–221.
Emile-Geay, J., McKay, N.P., Kaufman, D.S., Von Gunten, L., Wang, J., Anchukaitis, K.J., Abram, N.J., Addison, J.A., Curran, M.A., Evans, M.N., et al., 2017. A global multiproxy database for temperature reconstructions of the Common Era. Sci. Data 4, 170088.
Ferguson, C.W., Graybill, Da., 1983. Dendrochronology of bristlecone pine: a progress report. Radiocarbon 25, 287–288.
Frankson, R., Kunkel, K.E., Stevens, L.E., Easterling, D.R., 2019. 2017: New Mexico State Climate Summary (No. NOAA Technical Report NESDIS 149-NM).
Fritts, H., Lough, J., 1985. An estimate of average annual temperature variations for North America, 1602 to 1961. Clim. Change 7, 203–224.
Gilbert, E., Gries, C., Franz, N., Landrum, L.R., Nash I.I.I., T.H., 2019. SEINet: a centralized specimen resource managed by a distributed network of researchers. Biodivers. Inf. Sci. Stand.
Gonzalez, P., Garfin, G., Breshears, D., Brooks, K., Brown, H., Elias, E., Gunasekara, A., Huntly, N., Maldonado, J., Mantua, N., et al., 2018. Southwest. Impacts risks adapt. U. S. Fourth Natl. Clim. Assess. 2, 1101–1184.

Graumlich, L.J., 1993. A 1000-year record of temperature and precipitation in the Sierra Nevada. Quat. Res. 39, 249–255.
Gray, S.T., Fastie, C.L., Jackson, S.T., Betancourt, J.L., 2004. Tree-ring-based reconstruction of precipitation in the Bighorn Basin, Wyoming, since 1260 AD. J. Clim. 17, 3855–3865.
Hennig, C., 2007. Cluster-wise assessment of cluster stability. Comput. Stat. Data Anal. 52, 258–271.
Holmes, R.L., 1983. Computer-assisted quality control in tree-ring dating and measurement. Tree-Ring Bull.
Hu, J., Emile-Geay, J., Partin, J., 2017. Correlation-based interpretations of paleoclimate data–where statistics meet past climates. Earth Planet. Sci. Lett. 459, 362–371.
Hughes, M.K., Graumlich, L.J., 1996. Multimillennial dendroclimatic studies from the western United States. Climatic Variations and Forcing Mechanisms of the Last 2000 Years. Springer, pp. 109–124.
Jones, S.M., Gutzler, D.S., 2016. Spatial and seasonal variations in aridification across Southwest North America. J. Clim. 29, 4637–4649.
Kipfmueller, K.F., Salzer, M.W., 2010. Linear trend and climate response of five-needle pines in the western United States related to treeline proximity. Can. J. For. Res. 40, 134–142.
Knight, T.A., Meko, D.M., Baisan, C.H., 2010. A bimillennial-length tree-ring reconstruction of precipitation for the Tavaputs Plateau, Northeastern Utah. Quat. Res. 73, 107–117.
Körner, C., 2012. Alpine Treelines: Functional Ecology of the Global High Elevation Tree Limits. Springer Science & Business Media.
Krebs, P.V., 1973. Dendrochronology of bristlecone pine (Pinus aristata Engelm.) in Colorado. Arct. Alp. Res. 5, 149–150.
LaMarche Jr, V.C., Stockton, C.W., 1974. Chronologies from termperature-sensitive bristlecone pines at upper treeline in Western United States. Tree-Ring Bull.
Lehner, F., Wahl, E.R., Wood, A.W., Blatchford, D.B., Llewellyn, D., 2017. Assessing recent declines in Upper Rio Grande runoff efficiency from a paleoclimate perspective. Geophys. Res. Lett. 44, 4124–4133.
Meko, D.M., Woodhouse, C.A., 2011. Application of streamflow reconstruction to water resources management. Dendroclimatology. Springer, pp. 231–261.
Meko, D.M., Woodhouse, C.A., Baisan, C.A., Knight, T., Lukas, J.J., Hughes, M.K., Salzer, M.W., 2007. Medieval drought in the upper Colorado River Basin. Geophys. Res. Lett. 34.
Miller, K., 2014. 2,462 Years of Upper Arkansas River Basin Precipitation Reconstructed from Tree-rings at Black Mountain (Thesis). University of Arizona, Tucson, AZ.
Montes, J.R., Peláez, P., Willyard, A., Moreno-Letelier, A., Piñero, D., Gernandt, D.S., 2019. Phylogenetics of Pinus subsection cembroides engelm.(Pinaceae) inferred from low-copy nuclear gene sequences. Syst. Bot. 44, 501–518.
Overland, J.E., Preisendorfer, R., 1982. A significance test for principal components applied to a cyclone climatology. Mon. Weather Rev. 110, 1–4.
Preisendorfer, R.W., Mobley, C.D., 1988. Principal component analysis in meteorology and oceanography. Dev. Atmospheric Sci. 17.
Rehfeldt, G.E., Crookston, N.L., Warwell, M.V., Evans, J.S., 2006. Empirical analyses of plant-climate relationships for the western United States. Int. J. Plant Sci. 167, 1123–1150.
Richman, M.B., 1986. Rotation of principal components. J. Climatol. 6, 293–335.
Routson, C.C., Woodhouse, C.A., Overpeck, J.T., 2011. Second century megadrought in the Rio Grande headwaters, Colorado: how unusual was medieval drought? Geophys. Res. Lett. 38.
Salzer, M.W., Kipfmueller, K.F., 2005. Reconstructed temperature and precipitation on a millennial timescale from tree-rings in the southern Colorado Plateau. USA. Clim. Change 70, 465–487.
Salzer, M.W., Hughes, M.K., Bunn, A.G., Kipfmueller, K.F., 2009. Recent unprecedented tree-ring growth in bristlecone pine at the highest elevations and possible causes. Proc. Natl. Acad. Sci. 106, 20348–20353.
Salzer, M.W., Bunn, A.G., Graham, N.E., Hughes, M.K., 2014a. Five millennia of paleotemperature from tree-rings in the Great Basin. USA. Clim. Dyn. 42, 1517–1526.
Salzer, M.W., Larson, E.R., Bunn, A.G., Hughes, M.K., 2014b. Changing climate response in near-treeline bristlecone pine with elevation and aspect. Environ. Res. Lett. 9, 114007.
Salzer, M.W., Pearson, C.L., Baisan, C.H., 2019. Dating the methuselah walk bristlecone pine floating chronologies. Tree-Ring Res. 75, 61–66.
Sambuco, E., Mark, B.G., Patrick, N., DeGrand, J.Q., Porinchu, D.F., Reinemann, S.A., Baker, G., Box, J.E., 2020. Mountain temperature changes from embedded sensors spanning 2000m in Great Basin National Park, 2006-2018. Front. Earth Sci. 8, 292.
Schoettle, A.W., Coop, J.D., 2017. Range-wide conservation of Pinus aristata: a genetic collection with ecological context for proactive management today and resources for tomorrow. New For. 48, 181–199.
Schulman, E., 1954. Longevity under adversity in conifers. Science 119, 396–399.
Sheppard, P.R., Comrie, A.C., Packin, G.D., Angersbach, K., Hughes, M.K., 2002. The climate of the US Southwest. Clim. Chang. Res. Lett. 21, 219–238.
Stokes, M., Smiley, T., 1968. Introduction to Tree-ring Dating. University of Chicago. Chicago Press, IL.
Tang, G., Arnone I.I.I., J.A., 2013. Trends in surface air temperature and temperature extremes in the Great Basin during the 20th century from ground-based observations. J. Geophys. Res. Atmos. 118, 3579–3589.
Tran, T.J., Bruening, J.M., Bunn, A.G., Salzer, M.W., Weiss, S.B., 2017. Cluster analysis and topoclimate modeling to examine bristlecone pine tree-ring growth signals in the Great Basin. USA. Environ. Res. Lett. 12, 014007.
Trouet, V., Van Oldenborgh, G.J., 2013. KNMI Climate Explorer: a web-based research tool for high-resolution paleoclimatology. Tree-Ring Res. 69, 3–14.
Udall, B., Overpeck, J., 2017. The twenty-first century Colorado River hot drought and implications for the future. Water Resour. Res. 53, 2404–2418.
Vaganov, E.A., Hughes, M.K., Shashkin, A.V., 2006. Growth Dynamics of Conifer Tree Rings: Images of Past and Future Environments. Springer Science & Business Media.
Ward Jr, J.H., 1963. Hierarchical grouping to optimize an objective function. J. Am. Stat. Assoc. 58, 236–244.
Wigley, T.M., Briffa, K.R., Jones, P.D., 1984. On the average value of correlated time series, with applications in dendroclimatology and hydrometeorology. J. Clim. Appl. Meteorol. 23, 201–213.
Wiken, E., Nava, F.J., Griffith, G., 2011. North american terrestrial ecoregions—level III. Comm. Environ. Coop. Montr. Can. 149.
Wilson, R., Anchukaitis, K., Briffa, K.R., Büntgen, U., Cook, E., D'arrigo, R., Davi, N., Esper, J., Frank, D., Gunnarson, B., et al., 2016. Last millennium northern hemisphere summer temperatures from tree rings: part I: the long term context. Quat. Sci. Rev. 134, 1–18.
Woodhouse, C.A., Overpeck, J.T., 1998. 2000 years of drought variability in the central United States. Bull. Am. Meteorol. Soc. 79, 2693–2714.
Woodhouse, C.A., Gray, S.T., Meko, D.M., 2006. Updated streamflow reconstructions for the Upper Colorado River basin. Water Resour. Res. 42.
Woodhouse, C.A., Pederson, G.T., Gray, S.T., 2011. An 1800-yr record of decadal-scale hydroclimatic variability in the upper Arkansas River basin from bristlecone pine. Quat. Res. 75, 483–490.
Woodhouse, C.A., Stahle, D.W., Díaz, J.V., 2012. Rio Grande and Rio Conchos water supply variability over the past 500 years. Clim. Chang. Res. Lett. 51, 147–158.
Woodhouse, C.A., Pederson, G.T., Morino, K., McAfee, S.A., McCabe, G.J., 2016. Increasing influence of air temperature on upper Colorado River streamflow. Geophys. Res. Lett. 43, 2174–2181.
Ziaco, E., Biondi, F., Rossi, S., Deslauriers, A., 2016. Environmental drivers of cambial phenology in Great Basin bristlecone pine. Tree Physiol. 36, 818–831.